Inorganic Chemistry

Article

pubs.acs.org/IC

Effect of Axial Ligand, Spin State, and Hydrogen Bonding on the Inner-Sphere Reorganization Energies of Functional Models of Cytochrome P450

Sabyasachi Bandyopadhyay, Atanu Rana, Kaustuv Mittra, Subhra Samanta, Kushal Sengupta, and Abhishek Dey*

Indian Association for the Cultivation of Science, 2A & 2B Raja S. C. Mullick Road, Jadavpur, Kolkata, West Bengal 700032, India

Supporting Information

ABSTRACT: Using a combination of self-assembly and synthesis, bioinspired electrodes having dilute iron porphyrin active sites bound to axial thiolate and imidazole axial ligands are created atop self-assembled monolayers (SAMs). Resonance Raman data indicate that a picket fence architecture results in a high-spin (HS) ground state (GS) in these complexes and a hydrogen-bonding triazole architecture results in a low-spin (LS) ground state. The reorganization energies (λ) of these thiolate- and imidazole-bound iron porphyrin sites for both HS and LS states are experimentally determined. The λ of 5C HS imidazole and thiolate-bound iron porphyrin active sites are 10−16 kJ/mol, which are lower than their 6C LS counterparts. Density functional theory (DFT) calculations reproduce these data and indicate that the presence of significant electronic relaxation from the ligand system lowers the geometric relaxation and results in very low λ in these 5C HS active sites. These calculations indicate that loss of one-half a π bond during redox in a LS thiolate bound active site is responsible for its higher λ relative to a σ-donor ligand-like imidazole. Hydrogen bonding to the axial ligand leads to a significant increase in λ irrespective of the spin state of the iron center. The results suggest that while the hydrogen bonding to the thiolate in the 5C HS thiolate bound active site of cytochrome P450 (cyp450) shifts the potential up, resulting in a negative ΔG, it also increases λ resulting in an overall low barrier for the electron transfer process.

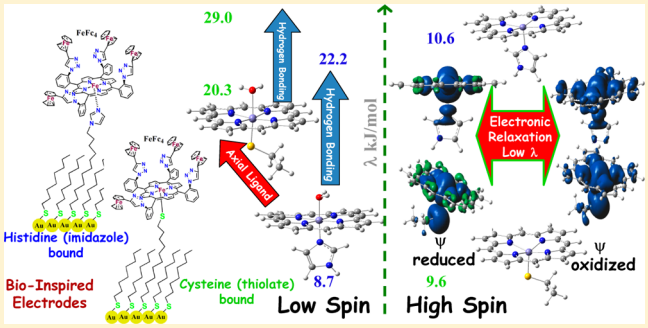

1. INTRODUCTION

Redox-active heme-based active sites catalyze vital life processes.[1,2] Depending upon the nature of the coordinating amino acid ligands and the substituent present in the porphyrin ring these cytochromes can be categorized as cytochrome *a*, *b*, *c*, *f*, and P450.[2,3] The Fe^{III}/Fe^{II} redox process is particularly important for these cytochromes and has been thoroughly investigated in cytochrome *a*, *b*, *c*, and *f*, where the low-spin (LS) six-coordinate (6C) heme active sites are involved in electron transport.[2,4−9] In general, these electron transfer (ET) active sites have neutral σ-donor axial ligands, e.g., histidine (imidazole headgroup), methionine (thioether headgroup), etc.[2] Apart from the 6C LS heme active sites involved in ET, the redox process is vital for the function of the five-coordinate (5C) high-spin (HS) heme active sites involved in O_2 activation, e.g., heme a_3 in cytochrome *c* oxidase (CcO) and cytochrome P450 (cyp450).[10−16] The ET rate from the reductase component reducing the inactive resting Fe^{III} form to the active Fe^{II} form plays a vital role in determining the kinetics of these active sites. In fact, in the cyp450 family of enzymes where the heme is bound via an axial cysteine (thiolate headgroup) ligand this ET process can even be the rate-determining step (rds) in catalysis.[17−19]

The kinetics of ET depends on several factors like the driving force (ΔG), reorganization energy (λ), and ET coupling element (H_{DA}).[2,20,21] A feature common to most ET sites in nature is a low λ. Cytochromes involved in ET possess very small λ (30−60 kJ/mol).[22,23] The total reorganization energy, λ, is the sum of the inner-sphere (λ_{is}) and outer-sphere (λ_{os}) components, i.e., $\lambda = \lambda_{is} + \lambda_{os}$.[2,20] λ_{os} is the energy change associated with the outer-sphere solvent shell surrounding the redox molecule.[2] Heme cofactors embedded in a protein active site have minimal λ_{os}. λ_{is} is the energy associated with the equilibrium internal bond vibrations of the redox molecule when the oxidation and reduction take place.[2,22] λ_{is} depends on the change in the bond lengths between the oxidized and the reduced states as expressed by eq 1.[22] The low λ_{is} of heme active sites in ET proteins is mainly due to efficient charge delocalization by the porphyrin ring of the hemin cofactor. This leads to very little change in bond lengths between the oxidized and the reduced states leading to lower λ_{is}

Received: May 15, 2014
Published: September 19, 2014

$$\lambda_{is} = \sum_i K_i \Delta r_i^2 \quad (1)$$

where K_i and Δr_i are the force constant and inner-sphere bond length changes, respectively, associated with the specific bonds of the respective species.

The active sites of cytochromes *a*, *b*, *c*, and *f*, which are involved in ET, bear neutral axial ligands like thioether and imidazole.[2,3] There are currently no experimental estimates of λ_{is} for the heme active sites bearing anionic axial ligands like thiolate, the coordinating side chain of the cysteine ligand of cyp450. Similarly, there is limited information available on the λ of the 5C HS active sites of CcO.[2,24] However, ET from their respective reductase components plays a vital role in the catalytic cycle. While in CcO ET from the adjacent heme a site to the catalytic heme a_3 site is very fast, in cyp450 ET from the reductase component is the rds in turnover.

In the past few years several bioinspired electrodes have been reported where both 5C HS[25,26] and 6C LS heme active sites bound to axial imidazole and thiolate ligands have been reported.[27,28] These electrodes not only efficiently reduced O_2 to H_2O under ambient conditions but also the thiolate-bound 5C HS iron porphyrin bearing bioinspired electrodes can utilize the high-valent intermediates formed during O_2 reduction to oxidize inert C−H bonds of cyclohexane with atmospheric O_2 in an aqueous medium with greater than 200 turnovers.[27] In this paper two different iron porphyrin complexes, α^4-tetra-2-(4-ferrocenyl-1,2,3-triazolyl)phenylporphyrinato Iron(II) ($FeFc_4$) and picket-fence Iron(II) porphyrin (FePf), are attached to two different SAMs, which result in imidazole-bound (Imd-SAM, Figure 1) and thiolate-bound (Thiol-SAM,

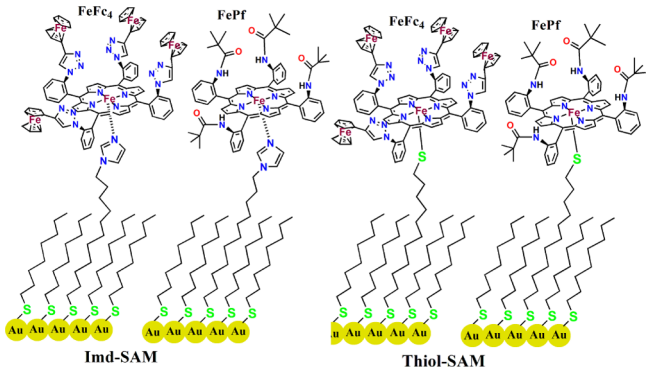

Figure 1. Pictorial representation of the catalysts $FeFc_4$ and FePf attached with Imd-SAM and Thiol-SAM.

Figure 1) iron porphyrin active sites at the same distance from the electrode. λ for the 5C HS and 6C LS iron porphyrin active sites having both imidazole and thiolate axial ligands are measured by determining the rate of ET at different temperatures.[29,30] λ for 5C HS species are determined to be very small relative to λ for a 6C LS species irrespective of the nature of the axial ligand (i.e., imidazole or thiolate). Furthermore, λ of LS thiolate-bound species is significantly more relative to a LS imidazole-bound species. These values are reproduced using geometry-optimized DFT calculations, and the nature of the axial ligand, spin state, and hydrogen-bonding interactions are found to tune λ_{is} significantly.

2. EXPERIMENTAL SECTION

Octanethiol (C_8SH) and potassium hexafluorophosphate (KPF_6) were purchased from Sigma-Aldrich. Disodium hydrogen phosphate dihydrate ($Na_2HPO_4{\cdot}2H_2O$) was purchased from Merck, and triethylamine (Et_3N) was purchased from Spectrochem India Pvt. Ltd. All reagents were used without any further purification. Gold (Au) wafers were purchased from Platypus Technologies (1000 Å of Au on 10 Å of a Ti adhesion layer on top of a Si(III) surface), and silver (Ag) discs for surface-enhanced resonance Raman spectroscopy (SERRS) experiments were purchased from Pine Instruments, U.S.A.

All electrochemical experiments were performed using a CH Instruments (CHI720D electrochemical analyzer). The platinum counter electrodes, Ag/AgCl (satd. KCl solution) reference electrodes, and Teflon plate material evaluating cell (ALS Japan) were purchased from CH Instruments. The SERRS experiments were performed using the Kr^+ laser (Sabre Innova, model SBRC-DBW-K) from Coherent, and a spectrograph (model Trivista555) fitted with an electronically cooled Pixis CCD from Princeton Instruments was used. The excitation wavelength used in the Raman experiments was 413.1 nm; the power applied on the surface was around 10−20 mW.

Detailed synthetic procedures of ImdC11SH, SHC11SH, and FeFc4 have already been reported.[27,31,32] FePf was synthesized as reported.[33] Preparation of the surfaces and functionalization of the SAM were done as previously reported.[27] Temperature-dependent CV experiments were done on Au wafers using degassed pH 7 buffer at three different temperatures, such as 277, 297, and 317 K, in an argon glovebox.

Ag discs were roughened following the reported procedure[34] and then immersed into the SAM solutions. The SERRS experiments were done by mounting the discs on a platinum ring disc assembly (Pine Instruments, U.S.A.). After attaching the catalyst the SAM-modified surfaces were immersed into the deoxygenated pH 7 buffer kept in a closed airtight cell fitted with an Ag/AgCl reference electrode and a Pt counter electrode. In SERRS experiments the oxidized (Ox) and reduced (Red) spectra were recorded by applying the potentials onto the surface at 0 and −0.5 V, respectively.

All DFT calculations were performed on the Inorganic-HPC cluster at IACS using the Gaussian 03 software[35] package. Geometries were optimized with the spin-unrestricted formalism using both the BP86 functional and the 6-311G* basis set.[36,37] Frequency calculations were performed on each optimized structure using the same basis set to ensure that it was a minimum on the potential energy surface.

3. RESULTS AND ANALYSIS

3.1. Experimental Investigations. *3.1.1. Cyclic Voltammetry (CV).* Cyclic voltammograms of the $FeFc_4$ catalyst attached on the Imd-SAM (Figure 1) and Thiol-SAM (Figure 1) are recorded in deoxygenated pH 7 buffer solution. Data show Fc^+/Fc and Fe^{III}/Fe^{II} redox processes (Figure 2 and S1, Supporting Information) consistent with previous results.[27] $E_{1/2}$ of the Fc^+/Fc and porphyrin Fe^{III}/Fe^{II} processes are obtained at 358 ± 8 and −214 ± 6 mV, respectively, for the Imd-SAM (Figure 2A and S1a, Supporting Information) and at 355 ± 10 and −240 ± 8 mV, respectively (Figure 2B and S1b, Supporting Information), for the Thiol-SAM. In the recent past, it has been established that the iron center of the $FeFc_4$ catalyst binds the Imd-SAM though the imidazole headgroup and the Thiol-SAM through an ionized thiolate headgroup under these experimental conditions.[27] Note that the Fc groups of $FeFc_4$ complex have no direct interaction with the imidazole or thiolate ligands of the respective SAMs. Thus, $E_{1/2}$ of the Fc^+/Fc process appears at the same potential irrespective of the axial ligand and serves as an internal redox standard for this system. Additionally, the integrated charge under the Fc^+/Fc process does not change during these measurements, indicating that there is no loss of the porphyrin complex during these

dx.doi.org/10.1021/ic501112a | Inorg. Chem. 2014, 53, 10150−10158

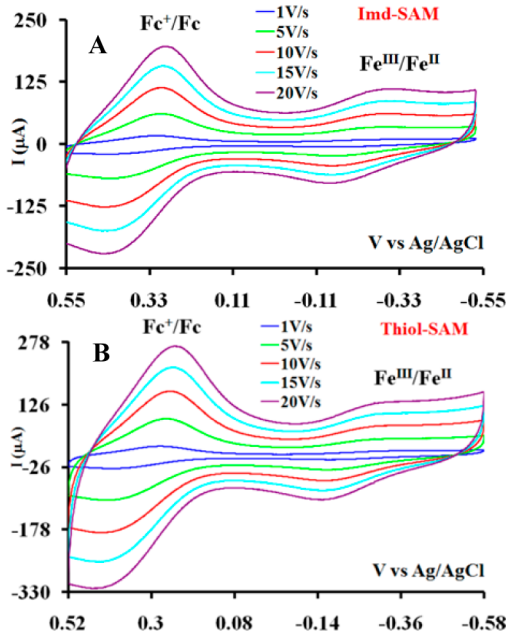

Figure 2. Cyclic voltammograms of $FeFc_4$-attached (A) Imd-SAM and (B) Thiol-SAM in different scan rates recorded at room temperature in pH 7 buffer using Ag/AgCl as reference electrode and Pt wire as counter electrode.

experiments. A noticeable difference in the electrochemical response of the $FeFc_4$ complex is that the extent of peak separation between the cathodic and the anodic processes (ΔE_p) is different for the Fc^+/Fc and the Fe^{III}/Fe^{II} processes between the Imd-SAM and the Thiol-SAM. The Thiol-SAM functionalized electrode shows much greater ΔE_p relative to the Imd-SAM-functionalized electrode. ΔE_p reflects the rate of ET from the electrode to the complex. Since the Fe center of the porphyrin is directly attached to the SAM through the imidazole or thiolate group, the distance of this redox-active center from the surface is likely to be the same. Hence, ΔE_p should not be affected by the distance of these centers from the electrode. Alternatively, the rate of ET can depend on the nature of the axial ligand to the iron. The increased ΔE_p on the Thiol-SAM likely reflects a slower rate of ET through a thiolate ligand relative to that through an imidazole ligand in the Imd-SAM.

For the FePf complex, the $Fe^{III/II}$ process is observed at −220 ± 7 and −248 ± 10 mV for the Imd-SAM and Thiol-SAM, respectively[27] (Figure S2, Supporting Information). Note that this complex does not bear the Fc groups present in the $FeFc_4$ complex, and hence, no Fc^+/Fc process is observed. The CV data obtained at different temperatures clearly indicate that ΔE_p is significantly higher for the Thiol-SAM-bound FePf relative to the Imd-SAM-bound FePf (Figure S2, Supporting Information). $E_{1/2}$ of the imidazole-bound $FeFc_4$ and FePf complexes is only ∼30 mV more positive in an aqueous medium than the corresponding thiolate-bound complexes due to OH^- coordination to the former. It is also important to note that the change in spin state does not seem to affect $E_{1/2}$.[38] This may seem inconsistent with results obtained in cyp450 enzymes, where $E_{1/2}$ is raised by 100−150 mV upon substrate binding which changes the GS of the resting ferric state from LS to HS.[39,40] However, unlike cyp450 where the reduced state has a HS GS irrespective of the GS of the oxidized state, the reduced state of thiolate-bound FePf is HS while that of $FeFc_4$ is LS (vide infra).

3.1.2. pH Dependence. Both the $FeFc_4$ and FePf catalysts which are attached to Imd-SAM show pH-dependent $E_{1/2}$ (Figure S3, Supporting Information, red) between pH 4 and pH 9.[27] Since the Fc^+/Fc process in the $FeFc_4$ complex is pH independent, any change in the $Fe^{III/II}$ $E_{1/2}$ is due to the presence of ionizable trans water-derived ligand. An approximately 60 mV shift in $E_{1/2}$ per unit shift in pH is observed between pH 6 and 8 for Imd-SAM-bound $FeFc_4$ and FePf complexes (Figure S3, Supporting Information, red) characteristic of a single proton-coupled ET (PCET)[41,42] process and consistent with an $Imd{-}Fe^{III}{-}OH + e^- + H^+ = Imd{-}Fe^{II}\ OH_2$ redox equilibrium. In the case of the Thiol-SAM, CV data of the $FeFc_4$ and FePf complex do not show pH dependence between pH 6 and 8 (Figure S3b, Supporting Information, green).

3.1.3. Surface-Enhanced Resonance Raman Spectroscopy (SERRS). SERRS spectra of both the FePf and the $FeFc_4$ complexes (Table 1) are obtained in pH 7 buffer by attaching

Table 1. RR Signatures of the Species Involved

	SAM	ν_4 (cm^{-1})	ν_2 (cm^{-1})	species
FePf	Imd-SAM	1364	1554	Fe^{III} HS
	Thiol-SAM	1364	1554	Fe^{III} HS
$FeFc_4$	Imd-SAM (0 V)	1369	1567	Fe^{III} LS
	Thiol-SAM (0 V)	1371	1568	Fe^{III} LS
	Imd-SAM (−0.5 V)	1358	1558	Fe^{II} LS
	Thiol-SAM (−0.5 V)	1358	1559	Fe^{II} LS

them with the Imd-SAM and Thiol-SAM.[27] SERRS data of FePf complex attached to the imidazole SAM as well as Thiol-SAM are shown to exist in the HS state[27,43,44](Figure S4, Supporting Information). SERRS data of $FeFc_4$ catalyst bound to Imd-SAM and Thiol-SAM are determined in pH 7 buffer applying anodic (0 V) and cathodic (−0.5 V) potentials on the electrode to generate the oxidized and reduced species, respectively (Table 1). SERRS data of the $FeFc_4$ complex bound to the Thiol-SAM (Figure 3, top) show the ν_4 and ν_2 bands at 1371 and 1568 cm^{-1}, respectively[43] (Figure 3, top, red and brown), when an anodic potential of 0 V is applied. These values indicate the presence of a LS Fe^{III} center. On applying a reducing potential at the electrode (−0.5 V) the ν_4 and ν_2 bands appeared at 1358 and 1559 cm^{-1},[43] respectively, (Figure 3, top, green), indicating the presence of a LS Fe^{II} center in the reduced state of the thiolate-bound $FeFc_4$ complex. In all of these cases the sixth axial ligand required to stabilize a LS ground state is likely the solvent, H_2O. SERRS data of the $FeFc_4$ complex-bound Imd-SAM surface (Figure 3, bottom) show the ν_4 and the ν_2 bands at 1369 and 1567 cm^{-1}, respectively, when the electrode is held at 0 V, indicating that the Fe in the complex exists in the LS Fe^{III} state (Figure 3, bottom, violet and orange).[43]Note that the ν_4 and ν_2 region of the oxidized species is broad, possibly indicating the presence of some HS Fe^{III} along with the LS species, whereas when a cathodic potential of −0.5 V is applied, the ν_4 and ν_2 bands shift to 1358 and 1558 cm^{-1}, respectively, indicating reduction of the LS Fe^{III} center to its LS Fe^{II} state[43] (Figure 3, bottom, blue).

In both of the above cases upon reoxidation of the reduced species by applying an anodic potential of 0 V the SERR spectra obtained are identical to that of the oxidized species in these cases, indicating that the redox process is chemically reversible

dx.doi.org/10.1021/ic501112a | Inorg. Chem. 2014, 53, 10150−10158

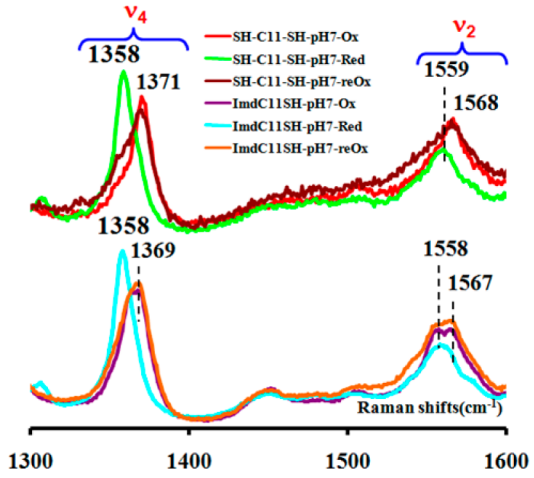

Figure 3. SERRS data of $FeFc_4$ attached to $ImdC_{11}SH$-C_8SH SAM (bottom) and $SHC_{11}SH$-C_8SH SAM (top). Data were recorded in pH 7 buffer using Ag/AgCl as reference electrode and Pt wire as counter electrode. Oxidized (Ox) and reduced (Red) spectra were taken by maintaining the potential at 0 and −0.5 V, respectively; reOx means reoxidized spectrum generated after oxidizing the reduced species.

under these conditions. Thus, the SERRS data indicate that while the FePf complex bound to imidazole and thiolate axial ligand mainly exists as a HS species, the $FeFc_4$ complex mainly exists as 6C LS species.[27] Further, the PCET process involved in both $FeFc_4$ and FePf bound to Imd-SAM suggests that there is OH^- ligand trans to the axial imidazole ligand in the ferric state.

3.1.4. Electron Transfer kinetics. The rate of heterogeneous ET (k_{app})[45,30,46] from the electrode to the iron porphyrin complexes[47−49] is determined using Laviron's method.[48,50−53] The separation between the oxidized and the reduced peak potentials (ΔE_p) at different scan rates (Figure 4 and S5, Supporting Information) is required to determine k_{app} using Laviron's approach.[51,52]

3.1.4.1. Apparent Rate Constant of ET (k_{app}). k_{app} of $FeFc_4$ and FePf is determined after attaching them to two different SAM surfaces such as Imd-SAM and Thiol-SAM through imidazole and thiolate linkages, respectively. Using Laviron's method from the cathodic and anodic peak potentials the

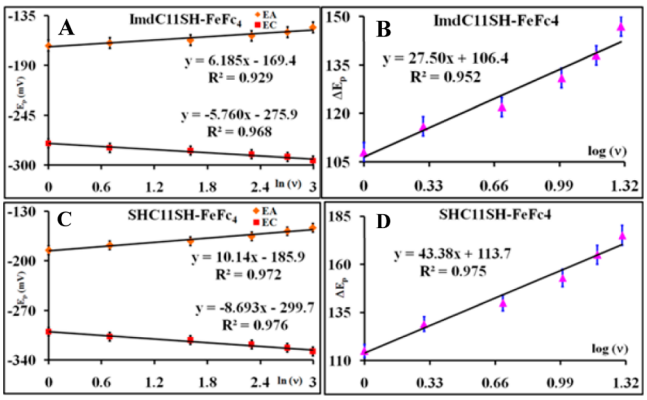

Figure 4. Plot of peak potential (E_p) vs ln(ν) for $FeFc_4$-attached (A) ImdC11SH-C8SH SAM and (C) SHC11SH-C8SH SAM in pH 7 buffer at room temperature. Plot of ΔE_p vs log (ν) for $FeFc_4$-attached (B) ImdC11SH-C8SH SAM and (D) SHC11SH-C8SH SAM at same condition. EA and EC are anodic and cathodic potentials, respectively.

transfer coefficient (α) can be determined using eqs 2 and 3, respectively[50−52]

$$E_{pc} = E - (RT/\alpha nF)\ln[\alpha/|m|] \quad (2)$$

$$E_{pa} = E + [RT/(1-\alpha)nF]\ln[(1-\alpha)/|m|] \quad (3)$$

where E_{pc} and E_{pa} are the cathodic and anodic peak potentials, respectively, and E is the formal potential of the redox-active species; here it is the $E_{1/2}$. R, T, n, and F have their usual meaning. From this formulation m can be designated as

$$m = (RT/F)(k_{app}/n\nu) \quad (4)$$

k_{app} is the apparent ET rate constant, ν is the scan rate in V/s, and $n = 1$.

Equations 2 and 3 can be simplified using eq 4 as

$$E_{pc} = E - (RT/\alpha nF)\ln[\alpha nF/RTk_{app}] - (RT/\alpha nF)\ln(\nu) \quad (5)$$

$$E_{pa} = E + [RT/(1-\alpha)nF]\ln[(1-\alpha)nF/RTk_{app}] + [RT/(1-\alpha)nF]\ln(\nu) \quad (6)$$

The plot of E_{pc} and E_{pa} with respect to ln(ν) is linear. The ratio of the slopes of the cathodic and anodic peak potentials yields the value of α (Figure 4 and S5, Supporting Information). Further, α values for the $FeFc_4$ and FePf complexes attached with two different SAM surfaces (Imd-SAM and Thiol-SAM) are determined at three different temperatures. Determination of k_{app} at different temperatures allows evaluation of the reorganization energies (vide infra). The result shows that the $FeFc_4$-attached Imd-SAM has α values of 0.46, 0.51, and 0.50 at 277, 297, and 317 K, respectively (Table 2).

Table 2. Experimentally Determined $E_{1/2}$, α, k_{app}, and λ of $FeFc_4$ and FePf Catalysts Attached to the $ImdC_{11}SH-C_8SH$ and $SHC_{11}SH-C_8SH$ SAM Surfaces

		α			
pH 7 buffer	$E_{1/2}$ (mV)	277 K	297 K	317 K	λ (kJ/mol)
$ImdC_{11}SH-FeFc_4$	−214 ± 6	0.46	0.51	0.50	29.0 ± 0.7
$SHC_{11}SH-FeFc_4$	−240 ± 8	0.53	0.52	0.56	23.2 ± 0.5
$ImdC_{11}SH-FePf$	−220 ± 7	0.48	0.48	0.55	10.6 ± 0.4
$SHC_{11}SH-FePf$	−248 ± 10	0.47	0.55	0.56	16.0 ± 0.8

k_{app} is determined using the equation

$$\log k_{app} = \alpha\log(1-\alpha) + (1-\alpha)\log\alpha - \log(RT/nF\nu) - \alpha(1-\alpha)nF\Delta E_p/2.3RT \quad (7)$$

$$\Delta E_p = 2.3RT/\alpha(1-\alpha)nF[\alpha\log(1-\alpha) + (1-\alpha)\log\alpha - \log(RT/nF\nu) - \log k_{app}] \quad (8)$$

where ΔE_p is the separation between the peak potentials.

The plot of ΔE_p versus log(ν) produced a straight line. k_{app} is determined from the intercept of this line. Using the values of α for the $FeFc_4$-attached SAM surfaces k_{app} values are calculated using eq 8 to be 5.35, 6.93, and 8.46 s^{-1} for Imd-SAM and 5.32, 6.40, and 7.74 s^{-1} for Thiol-SAM at 277, 297, and 317 K, respectively. Similarly, k_{app} of the FePf complex is determined to be 6.60, 7.64, and 8.12 s^{-1} for Imd-SAM and 4.3, 5.2, and

dx.doi.org/10.1021/ic501112a | Inorg. Chem. 2014, 53, 10150−10158

5.71 s^{-1} for Thiol-SAM, respectively, at 277, 297, and 317 K. Thus, the data clearly indicate that as the temperature increases ΔE_p of the iron porphyrin center of these complexes decreases and the k_{app} values increase.

3.1.4.2. Reorganization Energy (λ). The reorganization energy λ[21] is determined from the values of k_{app} determined at different temperatures.[30,51] The temperature dependence of the ET reaction can be understood using an Arrhenius plot of $\ln[k_{app}/T^{1/2}]$ vs T^{-1} (Figure 5) derived from the Marcus

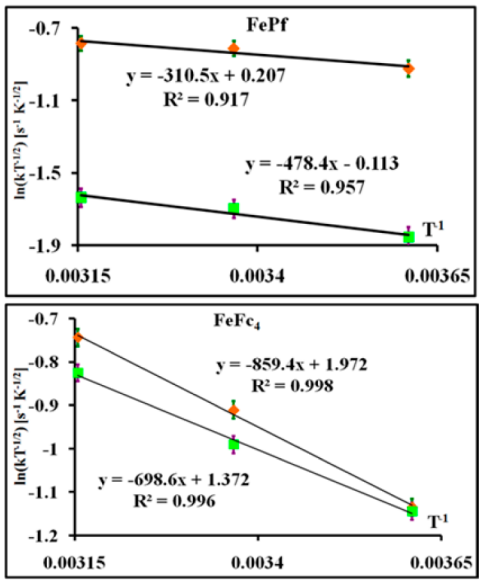

Figure 5. Arrhenius semilogarithmic plots of ($k_{app}T^{-1/2}$) vs $1/T$ for $FeFc_4$ and FePf-attached $ImdC_{11}SH-C_8SH$ SAM (Imd-SAM, orange) and $SHC_{11}SH-C_8SH$ SAM (Thiol-SAM, green).

density-of-states model applied for the ET process.[30,51] From the slope of the Arrhenius plot the value of λ can be determined assuming that λ is temperature independent. The reorganization energy can be calculated using the following equation

$$\lambda = -4.03\ \mathrm{d}\left(\ln[k_{app}/T^{1/2}]\right)/\mathrm{d}[T^{-1}] \quad (9)$$

The λ values are determined from the slope of the plot of $\mathrm{d}(\ln[k_{app}/T^{1/2}])/\mathrm{d}[T^{-1}]$[30,51]for the $FeFc_4$ and FePf complexes attached to Imd-SAM and Thiol-SAM (Figure 5). The $FeFc_4$ complex attached to Imd-SAM and Thiol-SAM has λ values of 29.0 ± 0.7 and 23.2 ± 0.5 kJ/mol, respectively (Table 2). Similarly, λ values for the FePf complex attached to Imid-SAM and Thiol-SAM are determined to be 10.6 ± 0.4 and 16.0 ± 0.8 kJ/mol, respectively (Table 2).

In summary, λ of the FePf and the $FeFc_4$ complexes attached to either Imd-SAM or Thiol-SAM is experimentally determined. λ, thus determined, represents the total λ (i.e., $\lambda_{is} + \lambda_{os}$). However, for sterically protected iron porphyrin complexes, λ_{os} can be very little; thus, the value of λ determined experimentally may represent mostly λ_{is}.[22] The experimental data indicate that λ values of the LS sites are, in general, higher than those of the HS sites. In the LS sites model the ET sites present in nature may be expected to have a lower λ. Thus, additional factors must be responsible in determining λ of these active sites, and these are analyzed using DFT calculations.

3.2. DFT Calculations. Experimental data allowed determination of λ for both 5C HS (FePf) and 6C LS ($FeFc_4$) iron porphyrin complexes with imidazole and thiolate as the axial ligands. DFT calculations[35−37] have been performed on a series of hypothetical complexes which vary in its axial ligation (imidazole vs thiolate), spin state (5C HS vs 6C LS), and hydrogen bonding (Figure 6, Table 3). Addition of an axial

II. DFT Calculations

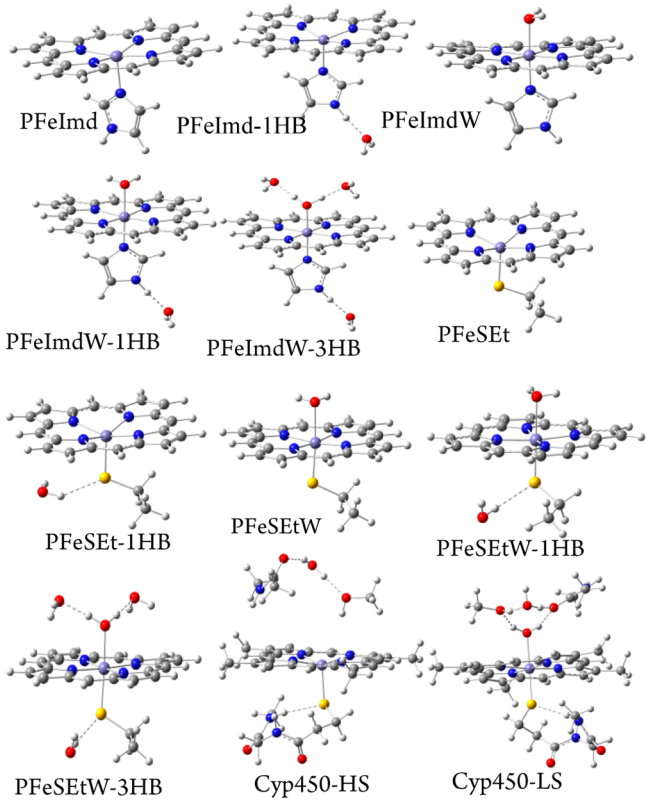

Figure 6. Structure of theoretically calculated iron porphyrin complexes and Cyp450. Dotted bonding represents the H bonding (HB): P = porphyrin moiety, Imd = imidazole, and W = water; red = oxygen, blue = nitrogen, yellow = sulfur, gray = carbon, and white = hydrogen.

water ligand to the imidazole-bound 5C HS model (PFeImd) results in the H_2O- and imidazole-bound LS model (PFeImdW). Introducing a hydrogen-bonding interaction from a water molecule to the bound imidazole ligand in the PFeImd model results in the PFeImd-1HB model. Addition of one hydrogen bond to the bound imidazole plus two hydrogen bonds to the bound H_2O ligand from noncoordinated H_2O molecules in the PFeImdW model results in the PFeImdW-1HB and PFeImdW-3HB models, respectively. The thiolate-bound (modeled by SEt) active site follows a similar nomenclature. Additionally, the geometries of the HS substrate-bound and LS resting active site of cyp450 have also been modeled (cyp450 HS and cyp450 LS in Figure 6). λ values of all these complexes are calculated and compared with the experimental results. λ can be classically related to the distortion of the geometry of a system during the ET process[2,22] (eq 1). Thus, a smaller change in the optimized geometries of the oxidized and reduced species can be expected to yield a smaller λ. The calculated λ values for the PFeImdW and PFeSEtW models are in good agreement with previous calculations by Ryde et al.[2]

The theoretically estimated λ_{is} values (Table 3) for the 5C HS PFeSEt and 6C LS PFeSEtW models are 9.6 and 20.3 kJ/

dx.doi.org/10.1021/ic501112a | Inorg. Chem. 2014, 53, 10150−10158

Table 3. Theoretically Predicted Δr and λ for Different Iron Porphyrin Models along with the Cytochrome P450 Model[a]

	Δr (pm)				
models	Fe−O_W	Fe−N_{imd}	Fe−S	Fe−N_P	λ (kJ/mol)
PFeImdW	5.2	-1.6	0.4		8.7 (**29.0**)
PFeImdW-1HB	4.3	0.5	0.3		8.7
PFeImdW-3HB	8.2	-0.3	0.7		22.2
PFeSEtW	8.6		10.0	1.3	20.3(**23.2**)
PFeSEtW-1HB	6.9		11.5	0.8	24.1
PFeSEtW-3HB	5.9		11.9	1.4	29.0
Cyp450-LS	4.5		10.3	1.8	47.3
PFeImd		5.0		1.3	10.6 (**10.6**)
PFeImd-1HB		5.4	1.1		12.5
PFeSEt	4.2	0.7			9.6 (**16.0**)
PFeSEt-1HB	3.1	0.7			14.5
Cyp450-HS			9.0	4.5	17.4

[a]HB = hydrogen bond, P = porphyrin, and W = water; LS = pink shade and HS = blue shade; experimental values in bold.

mol, respectively. These values are marginally lower than the experimental estimates (Table 2) of 16.0 ± 0.8 and 23.2 ± 0.5 kJ/mol for the thiolate-bound 5C HS FePf and the 6C LS $FeFc_4$ active sites, respectively. λ_{is} of an imidazole-bound 5C HS model is calculated to be 10.6 kJ/mol, which is remarkably close to the experimental value of 10.6 ± 0.4 kJ/mol for the imidazole-bound HS FePf active site. On the contrary, λ calculated for the PFeImdW model is 8.7 kJ/mol, which is significantly lower than the experimentally determined value of 29.0 ± 0.7 kJ/mol for the LS $FeFc_4$ complex. The deviation of the calculated λ_{is} for the imidazole-bound LS $FeFc_4$ complex from the computed value clearly indicates that there are additional contributions to the experimental value of λ, and these are considered below.

The experimental λ determined for the imidazole-bound LS iron porphyrin complex is 29 kJ/mol, which is indeed significantly larger than the λ value for a model without hydrogen bonding calculated here and elsewhere.[2,3] Note that the SERRS data show the presence of some HS contribution in the Imd-SAM $FeFc_4$ species (Figure 3). However, the HS λ_{is} (FePf) is 10.6 kJ/mol and does not explain the high λ for the Imd $FeFc_4$ complex. The pH dependence of $E_{1/2}$ for the imidazole-bound system clearly indicates that reduction of the imidazole-bound iron porphyrin complex is a PCET process.[27,41,42] λ_{is} of a PCET process can be approximately evaluated using Griffith's model[54−56] and is expressed as

$$\lambda_{is} = \sum_j \frac{f_j^r f_j^p}{f_j^r + f_j^p}(\Delta q_j)^2 \qquad (10)$$

λ_{is} is the summation of the individual contribution of the six (for LS) or five (for HS) Fe−ligand modes (j) which are assumed to be harmonic. The equilibrium force constants (K_i in eq 1) of the jth mode are designated as f_j^r and f_j^P for the reactant and product, respectively, and Δq_j (Δr_i in eq 1) is the difference in the reactant and product equilibrium bond lengths for the jth mode.[56]

In soybean lipoxyzenase the change of Fe−L bond lengths during a PCET redox process, involving a similar Fe^{III}−OH + $H^+ + e^- \rightarrow Fe^{II}$−$OH_2$ equilibrium, was greater than 0.2 Å and resulted in λ_{is} of 76 kJ/mol.[56] However, the optimized geometries (Table S2, Supporting Information) indicate that the Fe−N_{por} (N_{por} represents the pyrrolic nitrogen) and Fe−N_{imd} distances change by <0.02 Å during the redox process. Thus, the contribution to λ_{is} from these normal modes should be negligible as λ_{is} is directly proportional to the square of the change in bond length upon redox (eq 1). In the case of imidazole-bound FePf, the reduced state is HS 5C, i.e., the H_2O formed after protonation of the OH^- dissociates and thus the mode which contributed significantly to the λ_{is} in soybean lipoxygenase vanishes (the $f^p = 0$) in imidazole-bound FePf. This is why the experimental value of λ_{is} is very close to the theoretical estimate of the ET only value. However, this is not the case for the imidazole-bound $FeFc_4$ as its LS GS entails binding of the H_2O axial ligand in the reduced state. While the calculated changes in the Fe−N_{por} and Fe−N_{imd} bond lengths are negligible with the change of oxidation states (Table S2, Supporting Information), the Fe−OH_x mode can contribute to λ_{is} of this PCET process. This contribution to PCET can be roughly estimated using the calculated force constants (using the calculated vibrational frequencies) and the calculated change in distance (0.02 Å, Table S2, Supporting Information) to be 28.8 kJ/mol, which is very close to the experimental value obtained for the imidazole-bound LS $FeFc_4$ active site (29.0 kJ/mol). Note that a PCET process in a LS Os^{III} aquo complex was found to increase λ_{is} by 6.8 kJ/mol due to a change in the distance during the redox process between a covalently immobilized proton donor and a hydroxide ligand of a covalently immobilized Os center.[57] Such contributions are not likely to affect λ_{is} measured here as the proton donors are the solvent molecules which occupy the distal cavity due to noncovalent hydrogen bonding with the triazoles in $FeFc_4$.

When hydrogen bonding to the thiolate ligand (does not show PCET, Figure S3, Supporting Information, green) is modeled in these calculations, λ values increase to 24.1 and 14.5 kJ/mol from 20.3 and 9.6 kJ/mol for the 6C LS and the 5C HS thiolate-bound models, respectively (Table 3). These values are in reasonable agreement with the experimental data (23.2 and 16.0 kJ/mol for LS and HS, respectively, Table 2). Thus, successful modeling of the experimental λ values for a thiolate-bound iron porphyrin complex entails explicit inclusion of hydrogen-bonding interaction between the thiolate ligand and the water molecules of the solvent. Inclusion of H bonding to the axial water ligand (Figure 6, FePSEtW-3HB) increases the calculated λ_{is} from 24.1 (H bonding to thiolate only) to 29.0 kJ/mol (H bonding to thiolate and axial water molecules). The 5 kJ/mol increase of λ due to H bonding to the axial water ligand in the thiolate-bound models is significantly lower than the 14 kJ/mol increase calculated for the imidazole-bound model. This correlates well with the fact the change in the bond distances upon redox in the FePImdW-3HB relative to the FePImdW-1HB model is greater than the change in bond distances between the FePSEtW-3HB and the FePSEtW-1HB models. It is unclear at this point if the apparent disagreement between the calculated λ_{is} of the FePSEtW-3BH model and the experimental λ of $FeFc_4$ on thiol-SAM reflects inadequacies of the theoretical method or the hypothetical models used. The fact that the experimentally measured λ of the 5C thiolate- and imidazole-bound FePf and 6C imidazole-bound $FeFc_4$ can be

dx.doi.org/10.1021/ic501112a | Inorg. Chem. 2014, 53, 10150−10158

adequately reproduced in theory after including H bonding and PCET effects suggests that it is the latter.

In general, the calculated λ value increases with greater in change in bond length (Δr, eq 1) irrespective of the nature of the axial ligand, spin state of the metal, and extent of hydrogen bonding included in the model. For example, Δr for the PFeImdW model is lower than Δr of the PFeSEtW model, resulting in a lower λ in the former (Table 3), consistent with previous reports. The lower Δr for the imidazole-bound complex relative to that of a thiolate-bound complex can be explained by considering the differences in the nature of the RAMO (Figure 7)[58−60] involved in a LS iron porphyrin

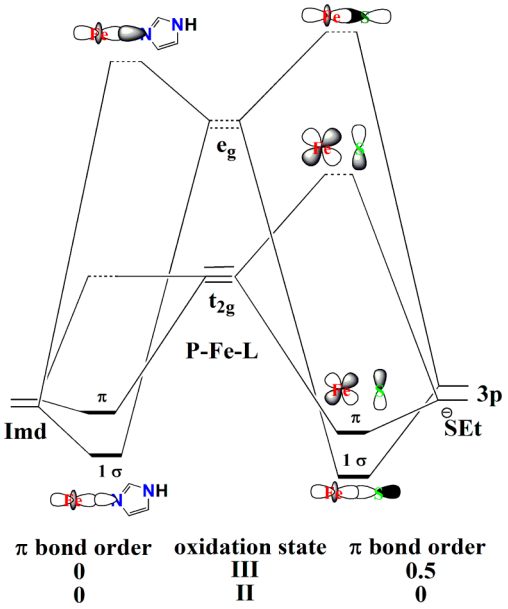

Figure 7. Redox-active molecular orbital (RAMO) diagram for Imd- and thiolate-bound Fe−P complexes.

complex having imidazole and thiolate axial ligands. Figure 7 shows that the singly occupied t_2 orbital is the RAMO involved in a $Fe^{III/II}$ process in a LS iron complex. Thiolate being a π-donor ligand utilizes this RAMO for π bonding with the Fe. The covalent bonding between the thiolate S_{3p} and the t_2 SOMO of the Fe^{III} center is clearly depicted in its contour. The donor thiolate S_{3p} orbital (the bonding orbital) being occupied, the singly occupied t_2 orbital (the antibonding orbital) provides a bond order of 0.5 to the Fe−S π bond. The σ bond involves the unoccupied d_{z^2} orbital (the antibonding orbital) and hence has a bond order of 1. As the RAMO is filled in the reduced Fe^{II} state (d^6 configuration) the π bond is lost, which results in significant elongation of the Fe−S bond. Thus, the redox process is associated with a change of Fe−S bond order of 0.5, which results in a large Δr of the Fe−S bond. Alternatively, imidazole does not have a very strong π bond with the t_2 orbital (mixing of imidazole nitrogen < 1%). Thus, in the case of imidazole, there is no change in iron imidazole bond order, which is why Δr of the iron imidazole bond is significantly less than that observed for the thiolate axial ligand in the LS state.

The calculated λ_{is} for thiolate-bound 5C HS iron porphyrin complex is 9.6 kJ/mol, which varies very little on changing the axial ligand from thiolate to imidazole. Thus, the large difference in λ between an imidazole-bound iron porphyrin and a thiolate-bound iron porphyrin in the LS state is not observed in the HS state. Figure 8 shows that the RAMO in the

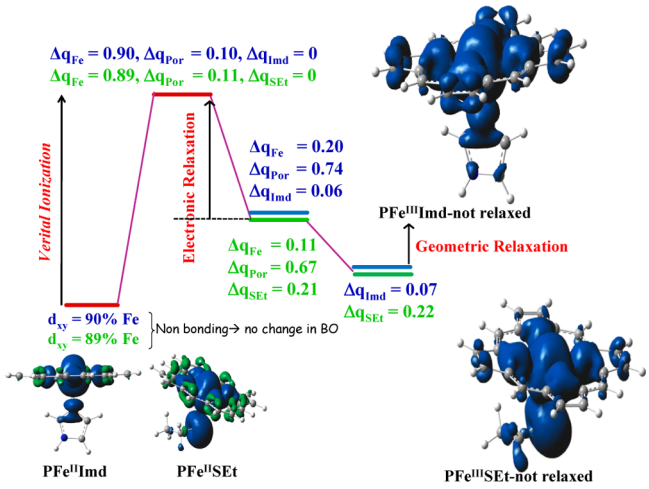

Figure 8. Spin density model for imidazole- and thiolate-bound Fe−porphyrin complexes in the HS state.

HS square pyramidal complexes is the d_{xy} orbital.[61] This orbital is nonbonding in nature, and the DFT-calculated wave functions for the PFeImd and PFeSEt models show 90% and 89% d_{xy} character, respectively. Thus, addition on one electron to this RAMO during reduction will reduce the Z_{eff} of the Fe by ∼0.9. This in turn will induce a large change in the geometry of the complex, resulting in large λ. However, the calculated wave functions for the reduced PFeImd and the PFeSEt complexes in their oxidized geometry (reduced relaxed in Table S1, Supporting Information) show very little change in the charge of the Fe center. In fact, the difference in electron densities of the oxidized and reduced wave functions in the PFeImd complex indicates that the electron density on the ring is increased by ∼0.74 e. The charge on the Fe center and on the imidazole axial ligand is increased by 0.20 and 0.06 e, respectively (Figure 8). Thus, ∼74% of the additional electron density gained during the reduction process is delocalized into the π orbitals of the ring, and only 20% is retained on the iron even when the geometry of the reduced PFeImd model is not allowed to relax. Further geometric relaxation (reduced in Table S1, Supporting Information) produced very little charge redistribution relative to the reduced relaxed state. Similar analysis of the reduction process of the PFeSEt model reveals that addition of one electron to the d_{xy} RAMO will lead to an increase of 0.9 e electron density on the Fe center. However, as the wave function is allowed to relax, keeping the geometry intact (reduced relaxed in Table S1, Supporting Information), the electron density on the Fe center increases by only 0.11. The rest is delocalized on the ligands. In addition to the π orbitals of the porphyrin ligand, the thiolate ligand aids the delocalization of the electron density of the reduced state significantly as its electron density increases by 0.21 e. Thus, only 11% of the additional charge gained upon reduction is retained on the Fe, 21% is delocalized on the thiolate, and the rest (∼67%) is delocalized on the porphyrin ligand. The wave function does not change significantly when the geometry of the reduced PFeSEt model is allowed to relax (reduced in Table S1, Supporting Information). Thus, large electronic relaxation owing to the delocalization of the additional charge density gained upon reduction into the porphyrin ligand (for PFeImD) and the axial thiolate ligand (for PFeSEt) reduces the change in geometry of this reduced state, thereby reducing λ_{is}.

dx.doi.org/10.1021/ic501112a | Inorg. Chem. 2014, 53, 10150−10158

4. DISCUSSION

The FePf and the $FeFc_4$ complexes allow determination of the ET rates and more specifically λ for the $Fe^{III/II}$ process with different biologically relevant axial ligands in both HS and LS states (Table 1). Additionally, the systems chosen helped investigate the effect of hydrogen bonding on λ. λ determined for these complexes varies between 10 and 30 kJ/mol (i.e., between 0.1 and 0.4 eV). The lowest λ are recorded for HS 5C thiolate- and imidazole-bound iron porphyrin complexes (10−16 kJ/mol). The LS 6C iron porphyrin complexes have λ on the order of 30 kJ/mol. There are several reports of λ for 6C LS iron porphyrin complexes and heme proteins, and the values are on the order of 70−90 and 40−60 kJ/mol, respectively.[18,22] The values of λ ($\lambda = \lambda_{is} + \lambda_{os}$) recorded in the active sites of protein are lower than those of complexes in solution due to reduction of the λ_{os} component in the protein active site, a key role played by the protein active site in lowering λ of these ET active sites.[22] The values of the imidazole- and thiolate-bound 6C LS active sites obtained using the $FeFc_4$ complex are 23−29 kJ/mol, which are very similar to those obtained for 6C LS ET sites. The solvent accessibility to the iron center in these complexes, which is sterically protected by the "picket" on one side and SAM on the other side, is thus minimal. Cytochrome *c* when attached to SAM shows a similar decrease in λ to 25 kJ/mol relative to its value of 40 kJ/mol in solution due to poorer access of solvent to the active site upon attachment of the protein on the surface.[8]

While reports of λ on 5C HS active site or complexes are scarce, Guiles reported a λ of 70 kJ/mol for hemoglobin.[62] The values obtained here are 10.6 and 16 kJ/mol using the FePf complex bound to imidazole and thiolate, respectively. Assuming that these complexes bear a sterically protected iron center has low λ_{os} contribution to λ as indicated above, these are the first experimental estimates of λ_{is} of HS 5C thiolate- and imidazole-bound iron porphyrin complexes. This may also suggest that there is significant λ_{os} contribution in the 5C HS hemoglobin active site; however, more analysis of this phenomenon is definitely warranted. DFT calculations indicate that the low λ_{is} of the HS 5C sites are derived from significant electronic relaxation (>70% of the charge density change during redox is localized on the π orbitals of the porphyrin ring, Figure 8) involved in the redox process which lowers the geometric relaxation keeping λ_{is} low. A similar reduction of λ due to the presence of an effective electronic relaxation process has been proposed for iron sulfur proteins.[59]

Theoretical estimations of λ_{is} of 6C LS iron porphyrin complexes with neutral Imd axial ligand agree well with previous estimates.[2] Additionally, these calculations indicate that the λ_{is} values of 6C LS thiolate-bound complexes are more than those of 6C LS imidazole-bound complexes. The higher λ_{is} of 6C LS thiolate-bound complexes correlates well with greater changes in Fe−S bond lengths in these complexes relative to their imidazole counterparts. This is due to the fact that the SOMO of a LS ferric center is a $d_{xz/yz}$ orbital, which is antibonding with respect to a π-donor ligand like thiolate. Reduction to the ferrous state entails occupying this antibonding orbital, which leads to loss of a π bond and elongation of the Fe−S bond length and results in increased λ_{is}.

The results and analysis presented here indicate that hydrogen-bonding interactions to the axial thiolate and water ligands result in an increase in λ. Inclusion of hydrogen bonding to the axial thiolate ligand is calculated to enhance λ_{is} by 40% and 20% in the 5C HS and 6C LS models, respectively. While the contribution of λ_{os} cannot be completely neglected in these experiments, these calculations indicate that inclusion of a hydrogen-bonding interaction alone resulted in λ_{is} values which are in reasonable agreement with the experimental results. Although there are no experimental data of the λ_{is} of cyp450, calculations indicate that λ_{is} of the 5C HS site is only 17.4 kJ/mol and that of the 6C LS is 47.3 kJ/mol. The former is very similar to the value experimentally determined for the 5C HS thiolate-bound FePf complex (16.0 kJ/mol) and that of the computational model PFeSEt-1HB-HS (14.5 kJ/mol) where one hydrogen bonding to the axial thiolate ligand is modeled. Note that the cyp450 active site is indeed characterized by the presence of a hydrogen-bonding interaction to the axial cysteine ligand.[63−65] λ_{is} for the 6C LS cyp450 site is calculated to be 47.3 kJ/mol, which is significantly more than that of the HS site due to the loss of 0.5 π bond order and presence of hydrogen bonding to the thiolate as well as the axial water ligand.

Thus, while hydrogen bonding raises the reduction potential it also increases λ_{is} by ∼8 kJ/mol (∼83 mV), i.e., from 9.6 kJ/mol in PFeSEt to 17.4 kJ/mol (∼180 mV) in cyp450 HS. This is likely to have an intriguing effect on ET barrier. ΔG of the ET between cyp450 in its substrate-bound 5C HS form and its reductase component is estimated to be −0.1 V.[66] Note that it is estimated that the conserved hydrogen-bonding shifts the formal potential of the 5C HS active site positive by 0.170 V, i.e., it is essential to result in a negative ΔG for the ET process.[67] However, the rate of ET varies exponentially with the sum of ΔG and λ ($\Delta G^{\ddagger} = (\Delta G + \lambda)^2/4\lambda k_B T$).[21] The contribution of λ_{is} to the exponent, enhanced due to hydrogen bonding, is estimated to be 0.18 V in the 5C HS substrate-bound state of cyp450. Thus, H bonding to the axial thiolate ligand in cyp450 not only raises the potential, resulting in a favorable ΔG for ET, but also is likely to raise λ opposing the negative ΔG for ET and minimize the exponent term in the ET rate.

■ ASSOCIATED CONTENT

Supporting Information

Additional SERRS data, CV data, and optimized geometries. This material is available free of charge via the Internet at http://pubs.acs.org.

■ AUTHOR INFORMATION

Corresponding Author

*E-mail: icad@iacs.res.in.

Notes

The authors declare no competing financial interest.

■ ACKNOWLEDGMENTS

This research was funded by DST SR/2009/IC-35 and SB/S1/IC-25/2013. S.B. acknowledges the IACS Int Ph.D. program.

■ REFERENCES

(1) Gray, H. B.; Winkler, J. R. *Biochim. Biophys. Acta* **2010**, *1797*, 1563−1572.

(2) Sigfridsson, E.; Olsson, M. H. M.; Ryde, U. *J. Phys. Chem. B* **2001**, *105*, 5546−5552.

(3) Jensen, K. P.; Ryde, U. *ChemBioChem* **2003**, *4*, 413−424.

(4) Pelletier, H.; Kraut, J. *Science (Washington, DC, U. S.)* **1992**, *258*, 1748−1755.

(5) Aedelroth, P.; Brzezinski, P.; Malmstroem, B. G. *Biochemistry* **1995**, *34*, 2844−2849.
(6) Zhang, Z.; Huang, L.; Shulmeister, V. M.; Chi, Y.-I.; Kim, K. K.; Hung, L.-W.; Crofts, A. R.; Berry, E. A.; Kim, S.-H. *Nature* **1998**, *392*, 677−684.
(7) Han, S. H.; Ching, Y. C.; Rousseau, D. L. *Proc. Natl. Acad. Sci. U.S.A.* **1990**, *87*, 8408−8412.
(8) Hildebrandt, P.; Murgida, D. H. *Bioelectrochemistry* **2002**, *55*, 139−143.
(9) Fraústo da Silvia, J. J. R. Williams, R. P. J. *The Biological Chemistry of the Elements*; Clarendon Press: Oxford, 1994.
(10) Yosca, T. H.; Rittle, J.; Krest, C. M.; Onderko, E. L.; Silakov, A.; Calixto, J. C.; Behan, R. K.; Green, M. T. *Science (Washington, DC, U. S.)* **2013**, *342*, 825−829.
(11) Makris, T. M.; Davydov, R.; Denisov, I. G.; Hoffman, B. M.; Sligar, S. G. *Drug Metab. Rev.* **2002**, *34*, 691−708.
(12) Jin, S.; Makris, T. M.; Bryson, T. A.; Sligar, S. G.; Dawson, J. H. *J. Am. Chem. Soc.* **2003**, *125*, 3406−3407.
(13) Kim, E.; Kamaraj, K.; Galliker, B.; Rubie, N. D.; Moanne-Loccoz, P.; Kaderli, S.; Zuberbahler, A. D.; Karlin, K. D. *Inorg. Chem.* **2005**, *44*, 1238−1247.
(14) Proshlyakov, D. A.; Pressler, M. A.; Babcock, G. T. *Proc. Natl. Acad. Sci. U.S.A.* **1998**, *95*, 8020−8025.
(15) Hosler, J. P.; Kim, Y.; Shapleigh, J.; Gennis, R.; Alben, J.; Ferguson-Miller, S.; Babcock, G. *J. Am. Chem. Soc.* **1994**, *116*, 5515−5516.
(16) Halime, Z.; Kotani, H.; Li, Y.; Fukuzumi, S.; Karlin, K. D. *Proc. Natl. Acad. Sci. U.S.A.* **2011**, *108*, 13990−13994.
(17) Guengerich, F. P. *Biol. Chem.* **2002**, *383*, 1553.
(18) Gray, H. B.; Winkler, J. R. *Annu. Rev. Biochem.* **1996**, *65*, 537−561.
(19) Yun, C.-H.; Miller, G. P.; Guengerich, F. P. *Biochemistry* **2000**, *39*, 11319−11329.
(20) Amashukeli, X.; Gruhn, N. E.; Lichtenberger, D. L.; Winkler, J. R.; Gray, H. B. *J. Am. Chem. Soc.* **2004**, *126*, 15566−15571.
(21) Marcus, R. A. *Annu. Rev. Phys. Chem.* **1964**, *15*, 155−196.
(22) Blankman, J. I.; Shahzad, N.; Dangi, B.; Miller, C. J.; Guiles, R. D. *Biochemistry* **2000**, *39*, 14799−14805.
(23) Muegge, I.; Qi, P. X.; Wand, A. J.; Chu, Z. T.; Warshel, A. *J. Phys. Chem. B* **1997**, *101*, 825−836.
(24) Battistuzzi, G.; Bellei, M.; Zederbauer, M.; Furtmaller, P. G.; Sola, M.; Obinger, C. *Biochemistry* **2006**, *45*, 12750−12755.
(25) Takahashi, S.; Wang, J.; Rousseau, D. L.; Ishikawa, K.; Yoshida, T.; Host, J. R.; Ikeda-Saito, M. *J. Biol. Chem.* **1994**, *269*, 1010−1014.
(26) Loew, G. H.; Harris, D. L. *Chem. Rev.* **2000**, *100*, 407−420.
(27) Sengupta, K.; Chatterjee, S.; Samanta, S.; Bandyopadhyay, S.; Dey, A. *Inorg. Chem.* **2013**, *52*, 2000−2014.
(28) Chatterjee, S.; Sengupta, K.; Samanta, S.; Das, P. K.; Dey, A. *Inorg. Chem.* **2013**, *52*, 9897−9907.
(29) Eckermann, A. L.; Feld, D. J.; Shaw, J. A.; Meade, T. J. *Coord. Chem. Rev.* **2010**, *254*, 1769−1802.
(30) Smalley, J. F.; Feldberg, S. W.; Chidsey, C. E. D.; Linford, M. R.; Newton, M. D.; Liu, Y.-P. *J. Phys. Chem.* **1995**, *99*, 13141−13149.
(31) Samanta, S.; Sengupta, K.; Mittra, K.; Bandyopadhyay, S.; Dey, A. *Chem. Commun.* **2012**, *48*, 7631−7633.
(32) Mittra, K.; Chatterjee, S.; Samanta, S.; Sengupta, K.; Bhattacharjee, H.; Dey, A. *Chem. Commun.* **2012**, *48*, 10535−10537.
(33) Collman, J. P.; Gagne, R. R.; Reed, C.; Halbert, T. R.; Lang, G.; Robinson, W. T. *J. Am. Chem. Soc.* **1975**, *97*, 1427−1439.
(34) Bryant, M. A.; Pemberton, J. E. *J. Am. Chem. Soc.* **1991**, *113*, 8284−8293.
(35) Frisch, M. J. T. et al. Gaussian, Inc.: Wallingford, CT, *Gaussian 03*, C.02; 2004.
(36) Perdew, J. P. *Phys. Rev. B* **1986**, *33*, 8822−8824.
(37) Becke, A. D. *Phys. Rev. A* **1988**, *38*, 3098−3100.
(38) Williams-Smith, D. L.; Cammack, R. *Biochim. Biophys. Acta* **1977**, *499*, 432−442.
(39) Sligar, S. G.; Gunsalus, I. C. *Biochemistry* **1979**, *18*, 2290−2295.
(40) Honeychurch, M. J.; Hill, H. A. O.; Wong, L.-L. *FEBS Lett.* **1999**, *451*, 351−353.
(41) Hammes-Schiffer, S.; Stuchebrukhov, A. A. *Chem. Rev.* **2010**, *110*, 6939−6960.
(42) Weinberg, D. R.; Gagliardi, C. J.; Hull, J. F.; Murphy, C. F.; Kent, C. A.; Westlake, B. C.; Paul, A.; Ess, D. H.; McCafferty, D. G.; Meyer, T. J. *Chem. Rev.* **2012**, *112*, 4016−4093.
(43) Burke, J. M.; Kincaid, J. R.; Peters, S.; Gagne, R. R.; Collman, J. P.; Spiro, T. G. *J. Am. Chem. Soc.* **1978**, *100*, 6083−6088.
(44) Hashimoto, S.; Mizutani, Y.; Tatsuno, Y.; Kitagawa, T. *J. Am. Chem. Soc.* **1991**, *113*, 6542−6549.
(45) The heterogeneous electron transfer (ET) rate can be determined by chronoamperometry (CA) where a current transient because of the potential step is plotted with respect to time. A single-exponential curve determines the ET rate of the respective monolayer species which produces a straight line for a semilogarithmic plot of this curve. The curve obtained with the $FeFc_4$ complex shows a deviation from the single-exponential behavior as this complex contains four ferrocene units which are within 7 Å of each other.
(46) Smalley, J. F.; Finklea, H. O.; Chidsey, C. E. D.; Linford, M. R.; Creager, S. E.; Ferraris, J. P.; Chalfant, K.; Zawodzinsk, T.; Feldberg, S. W.; Newton, M. D. *J. Am. Chem. Soc.* **2003**, *125*, 2004−2013.
(47) Clark, R. A.; Bowden, E. F. *Langmuir* **1997**, *13*, 559−565.
(48) Pilloud, D. L.; Chen, X.; Dutton, P. L.; Moser, C. C. *J. Phys. Chem. B* **2000**, *104*, 2868−2877.
(49) Wang, Q.; Zhi, F.; Wang, W.; Xia, X.; Liu, X.; Meng, F.; Song, Y.; Yang, C.; Lu, X. *J. Phys. Chem. C* **2009**, *113*, 9359−9367.
(50) Laviron, E. *J. Electroanal. Chem.* **1979**, *101*, 19−28.
(51) Park, W.; Hong, H. G. *Bull. Korean Chem. Soc.* **2006**, *27*, 381−385.
(52) Mhaske, S. D.; Ray, M.; Mazumdar, S. *Inorg. Chim. Acta* **2010**, *363*, 2804−2811.
(53) Weber, K.; Hockett, L.; Creager, S. *J. Phys. Chem. B* **1997**, *101*, 8286−8291.
(54) George, P.; Griffith, J. S. In *The Enzymes*; Boyer, P. D., Lardy, H., Myrback, K., Eds.; Academic Press: New York, 1959; Vol. *1*, Chapter 8, p 347.
(55) Zhou, Z.; Khan, S. U. M. *J. Phys. Chem.* **1989**, *93*, 5292−5295.
(56) Hatcher, E.; Soudackov, A. V.; Hammes-Schiffer, S. *J. Am. Chem. Soc.* **2004**, *126*, 5763−5775.
(57) Ludlow, M. K.; Soudackov, A. V.; Hammes-Schiffer, S. *J. Am. Chem. Soc.* **2010**, *132*, 1234−1235.
(58) Newton, M. D. *J. Phys. Chem.* **1988**, *92*, 3049−3056.
(59) Kennepohl, P.; Solomon, E. I. *Inorg. Chem.* **2003**, *42*, 696−708.
(60) Newton, M. D.; Ohta, K.; Zhong, E. *J. Phys. Chem.* **1991**, *95*, 2317−2326.
(61) Hu, C.; Sulok, C. D.; Paulat, F.; Lehnert, N.; Twigg, A. I.; Hendrich, M. P.; Schulz, C. E.; Scheidt, W. R. *J. Am. Chem. Soc.* **2010**, *132*, 3737−3750.
(62) Blankman, J. I.; Shahzad, N.; Miller, C. J.; Guiles, R. D. *Biochemistry* **2000**, *39*, 14806−14812.
(63) Denisov, I. G.; Makris, T. M.; Sligar, S. G.; Schlichting, I. *Chem. Rev.* **2005**, *105*, 2253−2278.
(64) Dey, A.; Okamura, T.-a.; Ueyama, N.; Hedman, B.; Hodgson, K. O.; Solomon, E. I. *J. Am. Chem. Soc.* **2005**, *127*, 12046−12053.
(65) Galinato, M. G. I.; Spolitak, T.; Ballou, D. P.; Lehnert, N. *Biochemistry* **2011**, *50*, 1053−1069.
(66) Munro, A. W.; Noble, M. A.; Robledo, L.; Daff, S. N.; Chapman, S. K. *Biochemistry* **2001**, *40*, 1956−1963.
(67) Dey, A.; Jiang, Y.; Ortiz de Montellano, P.; Hodgson, K. O.; Hedman, B.; Solomon, E. I. *J. Am. Chem. Soc.* **2009**, *131*, 7869−7878.